

Phase Behavior of 1-Dodecyl-3-methylimidazolium
Fluorohydrogenate Salts ($C_{12}MIm(FH)_nF$, $n = 1.0-2.3$)
and Their Anisotropic Ionic Conductivity as Ionic
Liquid Crystal Electrolytes

Fei Xu, Kazuhiko Matsumoto, and Rika Hagiwara*

Graduate School of Energy Science, Kyoto University, Yoshida, Sakyo-ku,

Kyoto 606-8501, Japan

* E-mail: k-matsumoto@energy.kyoto-u.ac.jp

Abstract

The effects of the HF composition, n , in 1-dodecyl-3-methylimidazolium fluorohydrogenate salts ($C_{12}MIm(FH)_nF$, $n = 1.0-2.3$) on their physicochemical and structural properties have been investigated using infrared spectroscopy, thermal analysis, polarized optical microscopy, X-ray diffraction, and anisotropic ionic conductivity measurements. The phase diagram of $C_{12}MIm(FH)_nF$ (n vs. transition temperature) suggests that $C_{12}MIm(FH)_nF$ is a mixed crystal system that has a boundary around $n = 1.9$. For all compositions, a liquid crystalline mesophase with a smectic A interdigitated bilayer structure is observed. The temperature range of the mesophase decreases with increasing n value (from 61.8 °C for $C_{12}MIm(FH)_{1.0}F$ to 37.0 °C for $C_{12}MIm(FH)_{2.3}F$). The layer spacing of the smectic structure decreases with increasing n value or increasing temperature. Two structural types with different layer spacings are observed in the crystalline phase (Type I, $1.0 \leq n \leq 1.9$, and Type II, $1.9 \leq n \leq 2.3$). Ionic conductivities parallel and perpendicular to the smectic layers (σ_{\parallel} and σ_{\perp}) increase with increasing n value, whereas the anisotropy of the ionic conductivities ($\sigma_{\parallel}/\sigma_{\perp}$) is independent of the n value, since the thickness of the insulating sheet formed by the dodecyl group remains nearly unchanged.

Keywords

Ionic liquids, Liquid crystals, Mesophases, Smectic

Introduction

Ionic liquid crystals (ILCs) have anisotropic structural organizations that are composed only of ionic species.¹ They are interesting candidates as one-dimensional²⁻⁴ or two-dimensional⁵⁻⁷ ion-conduction materials that can transport a specific ion and as anisotropic reaction media.⁸

Fluorohydrogenate ionic liquids are the liquids that can be formulated as $[\text{Cat}^+][(\text{FH})_n\text{F}^-]$, where $(\text{FH})_n\text{F}^-$ is the general expression for fluorohydrogenate anions such as FHF^- , $(\text{FH})_2\text{F}^-$, and $(\text{FH})_3\text{F}^-$.⁹⁻¹⁹ They have low melting points (*e.g.*, -60 °C for 1-ethyl-3-methylimidazolium fluorohydrogenate, $\text{EMIm}(\text{FH})_{2.3}\text{F}$), high ionic conductivities (100 mS cm^{-1} at 25 °C for $\text{EMIm}(\text{FH})_{2.3}\text{F}$), and low viscosities (4.9 cP at 25 °C for $\text{EMIm}(\text{FH})_{2.3}\text{F}$).¹⁰ Such properties make them attractive candidates as the electrolytes in various electrochemical devices such as electrochemical capacitors¹⁵ and fuel cells.^{13,20} We recently reported the fluorohydrogenate salts of cations with long alkyl chains, 1-alkyl-3-methylimidazolium ($\text{C}_x\text{MIm}(\text{FH})_2\text{F}$, $x = 8, 10, 12, 14, 16, \text{ and } 18$)²¹ and 1-alkyl-1-methylpyrrolidinium ($\text{C}_x\text{MPyr}(\text{FH})_2\text{F}$, $x = 10, 12, 14, 16, \text{ and } 18$).²² When an alkyl chain of appropriate length is introduced, they show a smectic A liquid crystalline mesophase around ambient temperature and exhibit a large anisotropy in ionic conductivity ($\sigma_{\parallel}/\sigma_{\perp} > 10$, where σ_{\parallel} and σ_{\perp} are the ionic conductivities parallel and perpendicular to the smectic layers). The highest ionic conductivity observed in this series of ILCs was 7.37 mS cm^{-1} at 25 °C for $\text{C}_{12}\text{MIm}(\text{FH})_2\text{F}$, which makes them potential electrolytes in electrochemical systems and processes including fluorohydrogenate fuel cells^{13,20} and electrochemical fluorination,²³ where the migration of $(\text{FH})_n\text{F}^-$ is involved in the electrode reactions.

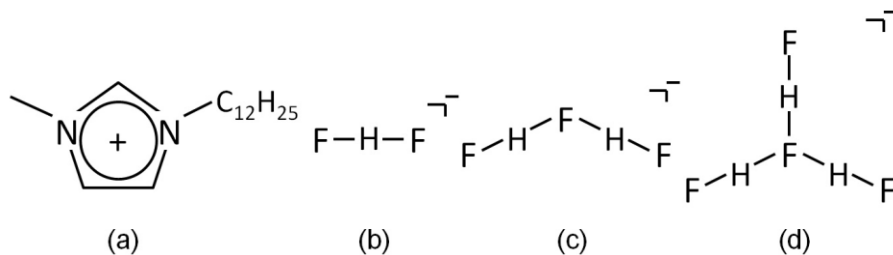
Fluorohydrogenate anions liberate HF at elevated temperatures,²⁴ although their salts are practically regarded to be nonvolatile after evacuation at the target temperature. Thermally stable fluorohydrogenate salts can be obtained by evacuation at high temperatures, which reduces the n value in $(\text{FH})_n\text{F}^-$.²⁴⁻²⁵ Investigation of effects of the n value on the properties of fluorohydrogenate ILCs is of significance as in the case of ionic liquids, because a wide operation temperature range extends the potential field of application of these ILCs.

In this study, a series of 1-dodecyl-3-methylimidazolium fluorohydrogenate ILCs ($\text{C}_{12}\text{MIm}(\text{FH})_n\text{F}$, $n = 1.0-2.3$) has been synthesized and characterized. The 1-dodecyl-3-methylimidazolium cation was

chosen because of the highest ionic conductivity and relatively low melting point of $C_{12}MIm(FH)_2F$ in the series of $C_xMIm(FH)_2F$ ($x = 10, 12, 14, 16, \text{ and } 18$) ILCs.²¹ The physicochemical properties and structures of the obtained fluorohydrogenate salts were studied by infrared (IR) spectroscopy, differential scanning calorimetry (DSC), polarized optical microscopy (POM), and X-ray diffraction (XRD). The anisotropic ionic conductivity parallel and perpendicular to the smectic layers was measured for the liquid crystalline mesophase.

Results and discussion

Synthesis and anionic structures. The vacuum-stable salt with the largest n value, $C_{12}MIm(FH)_{2.3}F$, was prepared by reaction of 1-dodecyl-3-methylimidazolium chloride and a large excess of anhydrous HF followed by evacuation (<1 Pa) at room temperature.^{9–11,15,26–27} The bifluoride salt, $C_{12}MIm(FH)_{1.0}F$, was prepared by reaction of $C_{12}MImOH$ and 1 M HF solution at a molar ratio of 1:2. The other $C_{12}MIm(FH)_nF$ salts with different n values were prepared by mixing $C_{12}MIm(FH)_{2.3}F$ and $C_{12}MIm(FH)_{1.0}F$ at a stoichiometric ratio, since the HF units are exchanged between the anions (see Scheme 1 for the structures of $C_{12}MIm^+$ and $(FH)_nF^-$). The IR spectra of the $(FH)_nF^-$ anion in $C_{12}MIm(HF)_nF$ (Figure S1, Supporting Information) are interpreted based on previous works.^{18,24} The $(FH)_2F^-$ anion shows broad absorption bands at ~ 450 , ~ 1050 , ~ 1800 , ~ 2000 , and ~ 2350 cm^{-1} .^{28–31} The intensities of these bands increase with increasing n value in the range of $1.0 \leq n \leq 2.0$ and decrease with increasing n value in the range of $2.0 \leq n \leq 2.3$. The broad absorption band at ~ 1250 cm^{-1} , whose intensity decreases with increasing n value, is ascribed to the fundamental mode, ν_3 , of FHF^- . The weak and broad absorption band at ~ 950 cm^{-1} , which is only observed for $C_{12}MIm(FH)_{2.3}F$, is ascribed to the $(FH)_3F^-$ anion. Consequently, the anionic species in $C_{12}MIm(FH)_nF$ ($n = 1.0–2.0$) are FHF^- and $(FH)_2F^-$, and those in $C_{12}MIm(HF)_nF$ ($n = 2.0–2.3$) are $(FH)_2F^-$ and $(FH)_3F^-$.^{18,24} The $C_{12}MIm(FH)_nF$ salts are waxy solids in the range of $1.0 \leq n \leq 1.7$ and viscous liquids in the range of $1.8 \leq n \leq 2.3$. The hygroscopicity of these fluorohydrogenate salts seems to decrease with increasing n value, which is confirmed by their weight uptake in air.



Scheme 1. Structures of (a) C₁₂MIm⁺, (b) FHF⁻, (c) (FH)₂F⁻, and (d) (FH)₃F⁻.

Table 1. Summary of the DSC analysis for C₁₂MIm(FH)_nF (*n* = 1.0–2.3)

<i>n</i>	<i>T_{tr}</i> ^a (°C)	<i>T_m</i> ^b (°C)	Δ <i>H</i> (kJ mol ⁻¹)	Δ <i>S</i> (J mol ⁻¹ K ⁻¹)	<i>T_c</i> ^c (°C)	Δ <i>H</i> (kJ mol ⁻¹)	Δ <i>S</i> (J mol ⁻¹ K ⁻¹)
1.0	-1.2	40.7	24.5	78.1	102.5	0.15	0.40
1.1	2.0	38.8	24.4	78.3	99.0	0.14	0.38
1.2	2.0	36.0	24.6	79.6	94.5	0.10	0.27
1.3	2.9	35.5	23.2	75.2	90.0	0.13	0.35
1.4	2.9	35.0	23.6	76.6	86.5	0.10	0.29
1.5	1.2	33.9	21.9	71.3	82.4	0.14	0.40
1.6	1.3	33.5	22.3	72.6	78.5	0.14	0.40
1.7	0.3	31.7	22.9	75.0	73.5	0.08	0.24
1.8	-2.8	28.8	21.3	70.6	69.5	0.13	0.38
1.9	-3.5	23.0	22.4	75.6	65.5	0.14	0.42
2.0	3.2	20.2	19.9	66.1	61.5	0.11	0.33
2.1	3.4	18.0	19.0	65.4	57.0	0.11	0.32
2.2	-8.2, 0.8 ^d	14.5	21.4	74.3	52.5	0.11	0.33
2.3	-6.6, 2.3 ^d	12.0	17.9	62.7	49.0	0.10	0.29

^aSolid-solid phase transition temperature. ^bMelting point. ^cClearing point. ^dTwo solid-solid phase transitions were observed for *n* = 2.2 and 2.3.

Thermal properties. Thermogravimetric (TG) analysis reveals that C₁₂MIm(FH)_nF decomposes around 230 °C regardless of the *n* value (Figure S2, Supporting Information). This behavior is similar to that of the other known C_xMIm(FH)_nF salts.²¹ For C₁₂MIm(FH)_nF with the *n* value lower than 1.8, a slight mass loss was observed around 100 °C, which was caused by evaporation of water absorbed just before the measurement. Figure 1 shows the DSC curves of C₁₂MIm(FH)_nF (*n* = 1.0, 1.5, 2.0, and 2.3;

see Figures S3–S5, Supporting Information, for the other n values), and Table 1 summarizes the DSC data (transition temperatures, ΔH , and ΔS). The endothermic peak with a large ΔH , which is ascribed to the breakup of a three-dimensionally ordered crystal lattice, corresponds to the melting point (from crystal to liquid crystal). The peak observed at a temperature higher than the melting point has a small ΔH and corresponds to the clearing point (from liquid crystal to isotropic liquid) where the breakup of an ordered structure mainly based on van der Waals interactions between alkyl chains occurs. The decrease in ΔH (and thus ΔS) at the melting point and clearing point with increasing n value can be explained by the decrease in the interaction between the anions and the imidazolium headgroups with increasing n value, since the anion becomes a weaker base as the size increases.

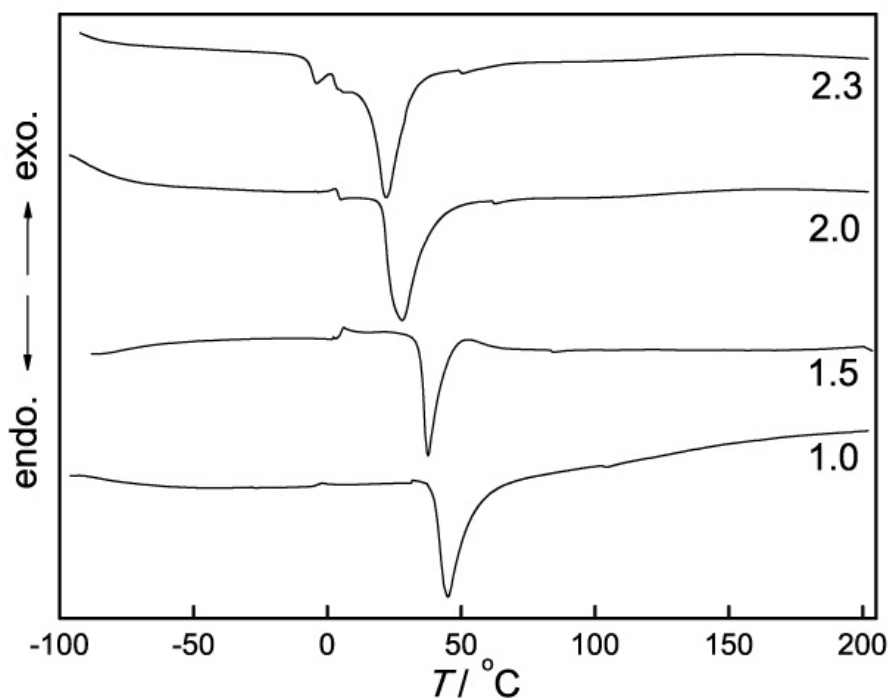


Figure 1. Differential scanning calorimetric curves (heating process) for $C_{12}MIm(FH)_nF$ ($n = 1.0, 1.5, 2.0,$ and 2.3).

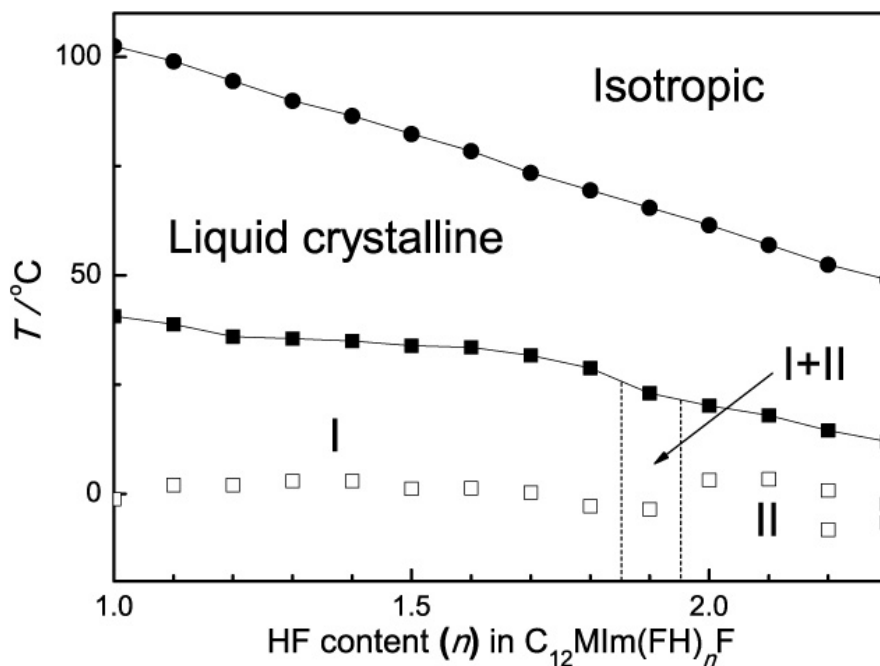


Figure 2. Phase diagram of $C_{12}MIm(FH)_nF$ (■: melting point; ●: clearing point; □: solid-solid phase transition temperature; I: crystalline phase Type I ($n = 1.0-1.8$); II: crystalline phase Type II ($n = 2.0-2.3$); I+II: mixture of Type I and Type II ($n = 1.9$)).

Figure 2 shows the phase transition temperatures of $C_{12}MIm(FH)_nF$ plotted as functions of n . Both the melting and clearing points decrease with increasing n value, while the clearing point shows a larger dependence (from 102.5 °C ($n = 1.0$) to 49.0 °C ($n = 2.3$)) than the melting point (from 40.7 °C ($n = 1.0$) to 12.0 °C ($n = 2.3$)), leading to a narrower temperature range of the liquid crystalline mesophase for $C_{12}MIm(FH)_nF$ ILCs with higher n values (e.g., 61.8 °C for $C_{12}MIm(FH)_{1.0}F$ and 37.0 °C for $C_{12}MIm(FH)_{2.3}F$). This trend is the same as that for ΔH and ΔS at the melting and clearing points due to the decrease in cation-anion interaction with increasing n value. When $C_{12}MIm(FH)_nF$ is compared with some other 1-dodecyl-3-methylimidazolium ILCs, the temperature range of the liquid crystalline mesophase follows the sequence of $Cl^- > Br^- > (FH)_{1.0}F^- > (FH)_{2.0}F^- > BF_4^- > SO_3CF_3^-$.³²⁻³⁴ Data on C_xMImAF_6 salts ($x = 14, 16, \text{ and } 18$; $A = P, As, Sb, Nb, \text{ and } Ta$) also suggest that the increase in the coulombic interaction between the imidazolium headgroup and the anion increases the temperature range

of the mesophase.³⁵ All the results above illustrate that the interaction within the polar region plays an important role in stabilizing the liquid crystalline mesophase.

Solid-solid phase transitions are observed for all the salts below melting point, and the transition temperature does not change significantly with increasing n value in the range of $1.0 \leq n \leq 1.9$. However, it rises at $n = 2.0$, and two solid-solid phase transitions are observed for $n = 2.2$ and 2.3 , suggesting that different crystal structures may form in the two ranges ($1.0 \leq n \leq 1.9$ and $2.3 \leq n \leq 1.9$).

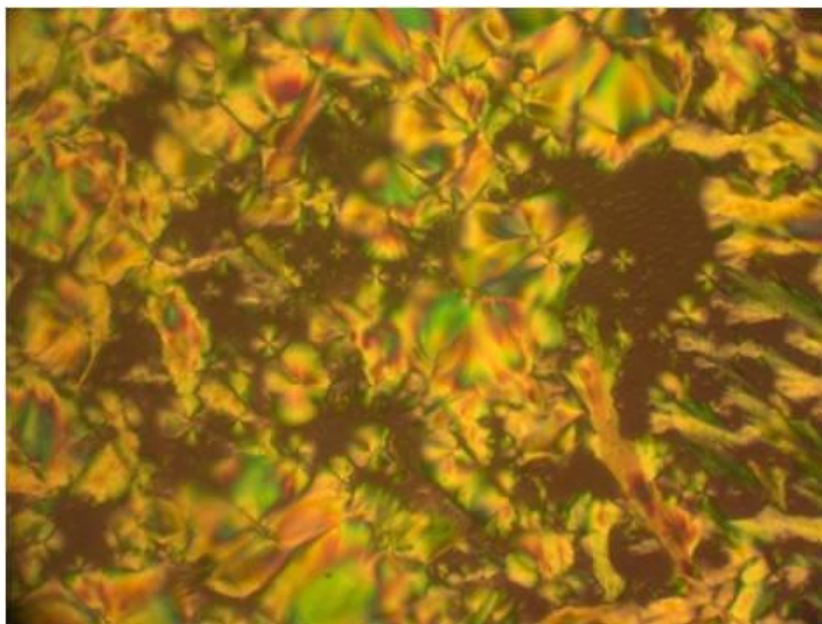


Figure 3. Polarized optical microscopic textures of $C_{12}MIm(FH)_{1.0}F$ at $50\text{ }^{\circ}C$.

Structural properties. Figure 3 shows the POM texture of $C_{12}MIm(FH)_{1.0}F$ at $50\text{ }^{\circ}C$ (see Figure S6 in Supporting Information for $n = 1.5$, 2.0 , and 2.3). Smooth fan-like textures grown from small batonnets ($n = 1.5$ and 2.0) or focal conic textures ($n = 2.3$) along with homeotropic regions ($n = 1.0$), indicative of smectic A mesophase, were observed for $C_{12}MIm(FH)_nF$. Variation of the n value does not change the type of liquid crystalline mesophase, and the texture for a smectic A mesophase was observed in all cases, which suggests that the large cation dominates the structure of the mesophase. The absence of the smectic C mesophase was confirmed, since broken fan-like texture was not observed in the liquid crystalline mesophase upon cooling from the isotropic phase.^{21,36} All the 1-alkyl-3-methylimidazolium ILCs reported until now show the same type of mesophase.^{1,21,35,37}

Figure 4 shows XRD patterns of $C_{12}MIm(FH)_nF$ ($n = 1.0, 1.3, 1.5, 1.8, 2.0, \text{ and } 2.3$) in the liquid crystalline mesophase at $40\text{ }^\circ\text{C}$ ($2^\circ < 2\theta < 6^\circ$; see Figure S7 in Supporting Information for the XRD patterns in the high-angle region, $2^\circ < 2\theta < 30^\circ$). Sharp peaks in the low-angle region indicate the formation of a layered structure. The absence of additional peaks in the high-angle region ($6^\circ < 2\theta < 30^\circ$) suggests the loss of positional ordering within the smectic layer plane (Figure S7, Supporting Information), which fits the characteristics of smectic A mesophase. Figure 5 shows the layer spacings of $C_{12}MIm(FH)_nF$ ($n = 1.0, 1.3, 1.5, 1.8, 2.0, \text{ and } 2.3$) as functions of temperature in the liquid crystalline mesophase, and Table S2 lists the values at each temperature. The layer spacing of the liquid crystalline mesophase decreases with increasing temperature, which is indicative of the smectic A_2 interdigitated bilayer structure.^{21,38}

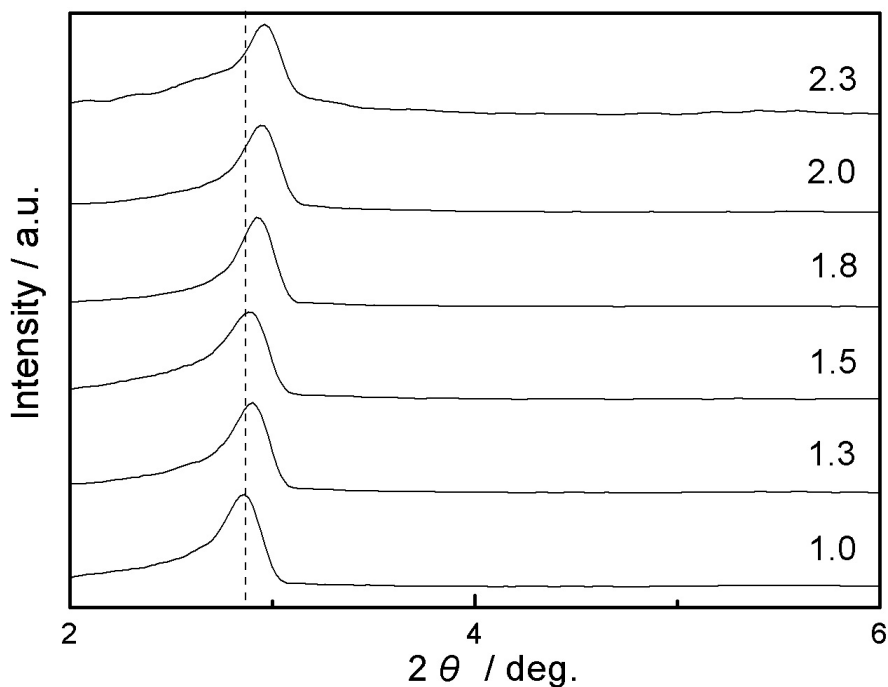


Figure 4. X-ray diffraction patterns of $C_{12}MIm(FH)_nF$ ($n = 1.0, 1.3, 1.5, 1.8, 2.0, \text{ and } 2.3$) at $40\text{ }^\circ\text{C}$ in the liquid crystalline mesophase.

As shown in Figures 4 and 5, the peak shifts toward the high-angle region with increasing n value, which indicates a decrease in the layer spacing in spite of the increase in size of the anion (volumes based on the MP2/aug-cc-pVTZ calculation: 47 \AA^3 for FHF^- , 63 \AA^3 for $(FH)_2F^-$, and 84 \AA^3 for

(FH)₃F⁻).¹⁸ Similar phenomena were also observed in an investigation of the layer spacings of a series of C_xMImAF₆ salts ($x = 14, 16, \text{ and } 18$; A = P, As, Sb, Nb, and Ta).³⁵ The layer spacing for the smectic A₂ liquid crystalline mesophase of other 1-alkyl-3-methylimidazolium salts also decreases as the size of the anion increases (Cl⁻ > Br⁻ > FHF⁻ > (FH)₂F⁻ > BF₄⁻ > SO₃CF₃⁻).^{21,38} The decrease in cation-anion interaction leads to a loose structure in the polar region and facilitates interdigitation of the alkyl chains, leading to the decrease in the layer spacing. A broadening of the peak was also observed with increasing n value (Figure 4), suggesting that the decrease in the interaction in the polar layer also lowers the degree of ordering of the layer structure.

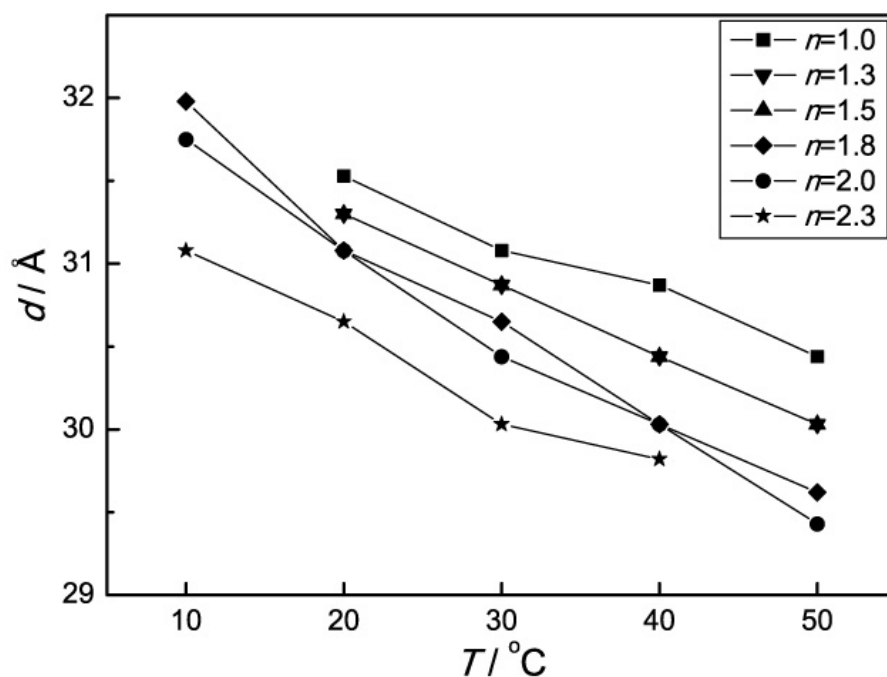


Figure 5. Layer spacings of C₁₂MIm(FH)_nF ($n = 1.0, 1.3, 1.5, 1.8, 2.0, \text{ and } 2.3$) in the liquid crystalline mesophase.

Figure 6 shows XRD patterns of C₁₂MIm(FH)_nF ($n = 1.0, 1.3, 1.5, 1.8, 1.9, 2.0, \text{ and } 2.3$) in the crystalline phase at -40 °C. For a small alkyimidazolium cation such as EMIm⁺, the crystalline phase of the fluorohydrogenate salt contains discrete anions such as FHF⁻ and (FH)₂F⁻, and salts with non-integer n values are mixtures of two salts containing these anions.^{18,24,27,39-41} On the other hand, C₁₂MIm⁺ shows significantly different behavior because of its bilayer structure. The C₁₂MIm(FH)_nF salts in the range of

$1.0 \leq n \leq 1.8$ have similar XRD patterns, suggesting the formation of the same type of structure (Type I). A completely different XRD pattern was observed for $C_{12}MIm(FH)_{2.0}F$ and $C_{12}MIm(FH)_{2.3}F$ (Type II) compared to those of $C_{12}MIm(FH)_nF$ with $1.0 \leq n \leq 1.8$. From the XRD pattern, $C_{12}MIm(FH)_{1.9}F$ is a mixture of $C_{12}MIm(FH)_{2.0}F$ and $C_{12}MIm(FH)_{1.8}F$. The phase diagram of $C_{12}MIm(FH)_nF$ ($n = 1.0-2.3$) is drawn in light of these observations (Figure 2), and it is interpreted as a mixed crystal system that has a boundary around $n = 1.9$. This also agrees well with the results of DSC: different solid-solid phase transition temperatures are observed for $n = 1.0-1.9$ and $n = 2.0-2.3$.

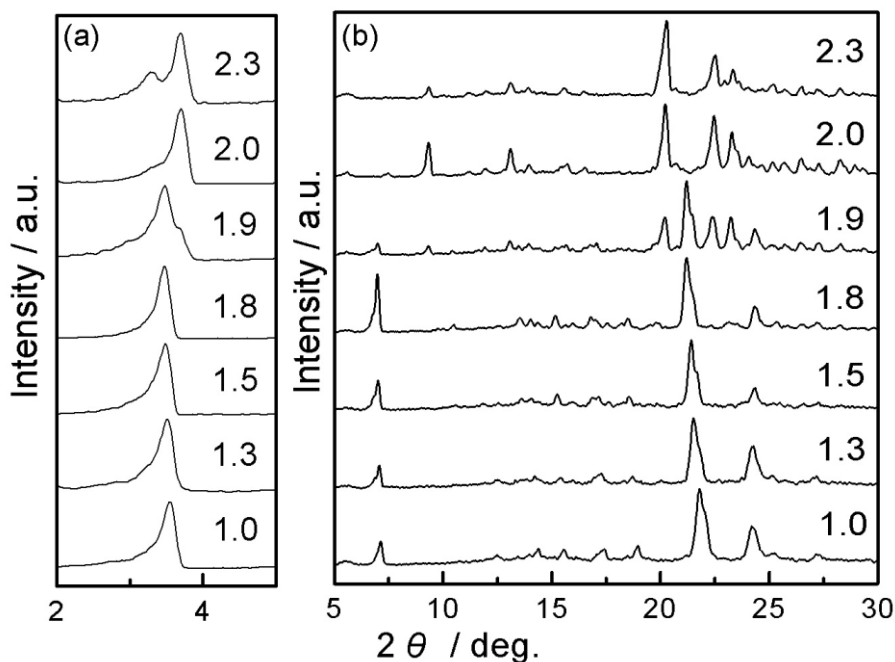


Figure 6. X-ray diffraction patterns of $C_{12}MIm(FH)_nF$ ($n = 1.0, 1.3, 1.5, 1.8, 1.9, 2.0,$ and 2.3) at $-40\text{ }^\circ\text{C}$ in the crystalline phase ((a) $2^\circ < 2\theta < 5^\circ$ and (b) $5^\circ < 2\theta < 30^\circ$).

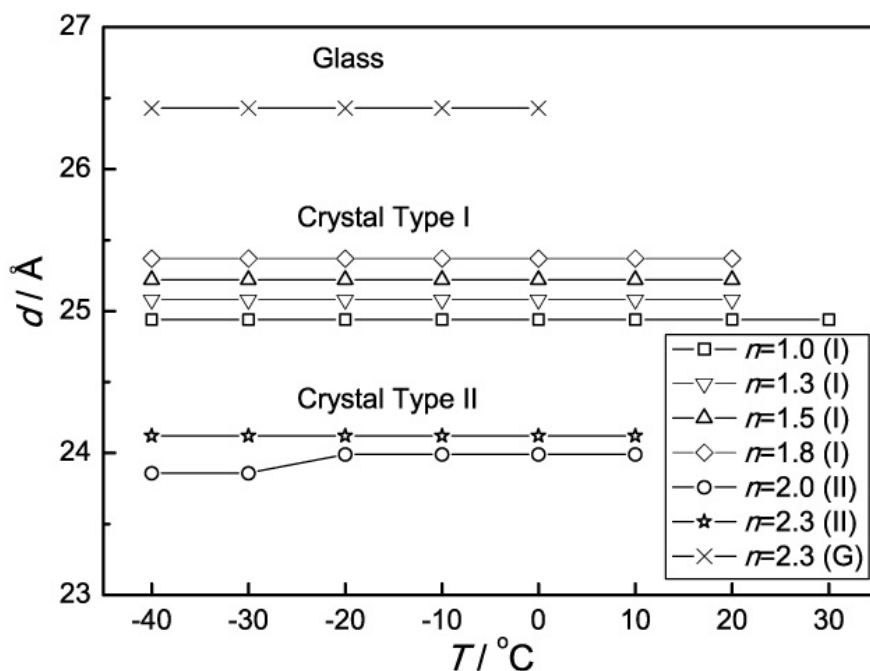


Figure 7. Layer spacings of $C_{12}MIm(FH)_nF$ ($n = 1.0, 1.3, 1.5, 1.8, 2.0,$ and 2.3) in crystalline phase Type I ($n = 1.0, 1.3, 1.5,$ and 1.8), crystalline phase Type II ($n = 2.0$ and 2.3), and the glassy phase ($n = 2.3$).

Figure 7 shows the layer spacings of $C_{12}MIm(FH)_nF$ ($n = 1.0, 1.3, 1.5, 1.8, 2.0,$ and 2.3) as functions of temperature for crystal Type I, $C_{12}MIm(FH)_nF$ ($n = 1.0-1.8$); crystal Type II, $C_{12}MIm(FH)_nF$ ($n = 2.0-2.3$); and the glassy phase (see Table S2 for the layer spacings at each temperature). In contrast to the liquid crystalline mesophase, the solid phase has a layer spacing that is insensitive to temperature. It is likely that the chains of the cations are tilted with respect to the layer plane or interdigitate more deeply in the crystalline phase,^{21,35,38} because smaller layer spacings are observed in the crystalline phase than in the liquid crystalline mesophase. The two layer spacings observed in the solid phase of $C_{12}MIm(FH)_{2.3}F$ are assigned to the glassy phase from the liquid crystalline mesophase ($2\theta = 3.3^\circ$) and the crystalline phase ($2\theta = 3.7^\circ$). The layer spacing for the glassy phase of $C_{12}MIm(FH)_{2.3}F$ is 26.4 \AA , while those for the Type I and Type II structures are about 25 and 24 \AA , respectively. Both of these layer spacings increase slightly with increasing n value, which indicates that the lattice parameters increase along with the increase in anion size. According to the previous work, the crystal structure of

$C_{18}MImAF_6$ salts ($A = P, As, Sb, Nb,$ and Ta) can be described as a layered structure of polar and nonpolar domains.³⁵ The sheets consisting of the NaCl-type located imidazolium headgroups and AF_6^- anions (polar domains) are separated by tilted interdigitated alkyl chains (nonpolar domains). An increase in the anion size results in an increase in the distance between the alkyl chains, since the anions and imidazolium headgroups are located in the same layers. This causes an increase in the overlapping alkyl chain length and a decrease in the layer spacing. Here, the $C_{12}MIm(FH)_nF$ salt shows a different trend. The layer spacing of $C_{12}MIm(FH)_nF$ in both Type I ($n = 1.0-1.8$) and Type II ($n = 2.0-2.3$) structures increases with increasing n value (and thus increasing anion size), suggesting that the configuration of the anions and imidazolium headgroups may be different from those of $C_{18}MImAF_6$ salts. This means that the slight increase in layer spacing with increasing n value could be solely ascribed to the increase in the anion size.¹⁸

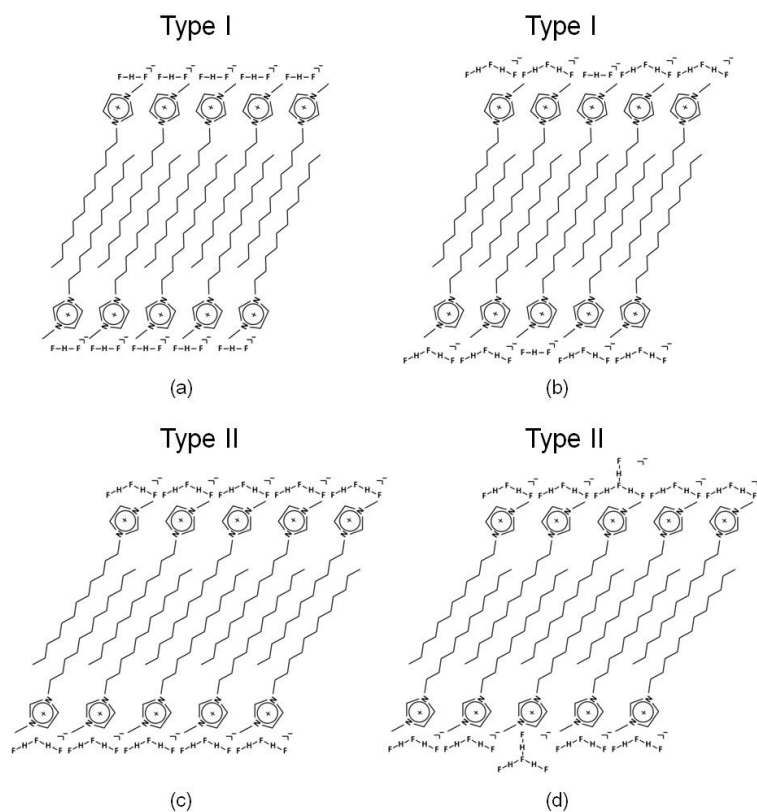


Figure 8. Schematic drawing of the structure of the crystalline phase for (a) $C_{12}MIm(FH)_{1.0}F$ (Type I), (b) $C_{12}MIm(FH)_{1.8}F$ (Type I), (c) $C_{12}MIm(FH)_{2.0}F$ (Type II), and (d) $C_{12}MIm(FH)_{2.2}F$ (Type II).

Figure 8 shows a schematic drawing of the crystalline phase for $C_{12}MIm(FH)_nF$ (Type I: (a) $n = 1.0$ and (b) $n = 1.8$; Type II: (c) $n = 2.0$ and (d) $n = 2.2$). The increase in anion size (from FHF^- to $(FH)_2F^-$) increases the layer spacing without changing the type of crystal structure from $n = 1.0$ to 1.8. The Type I structure can only accept $(FH)_2F^-$ up to $n = 1.8$ and transforms to Type II at $n = 1.9$. It is likely the alkyl chains tilt or interdigitate more in the Type II structure ($n = 2.0$ – 2.3) than in Type I ($n = 1.0$ – 1.8), since small layer spacings are observed in spite of the larger counteranions.

Anisotropic ionic conductivity. The ionic conductivities parallel (σ_{\parallel}) and perpendicular (σ_{\perp}) to the smectic layer were measured for $C_{12}MIm(FH)_nF$ ($n = 1.0, 1.3, 1.5, 1.8, \text{ and } 2.0$) in the liquid crystalline mesophase. Focal conic textures along with pseudo-isotropic domains were observed when the sample was placed in the conductivity measurement cell and heated up to the liquid crystalline mesophase. Homeotropic alignment of these fluorohydrogenate ILCs was achieved by simply applying pressure on the cover glass, which was confirmed by the unchanged view under crossed Nicol prisms when the sample holder was rotated.³⁶ Cooling down from the isotropic phase or shearing in the liquid crystalline mesophase^{2–6} is not necessary for the alignment of the ILCs, probably because of their simple structures and relatively low viscosity.

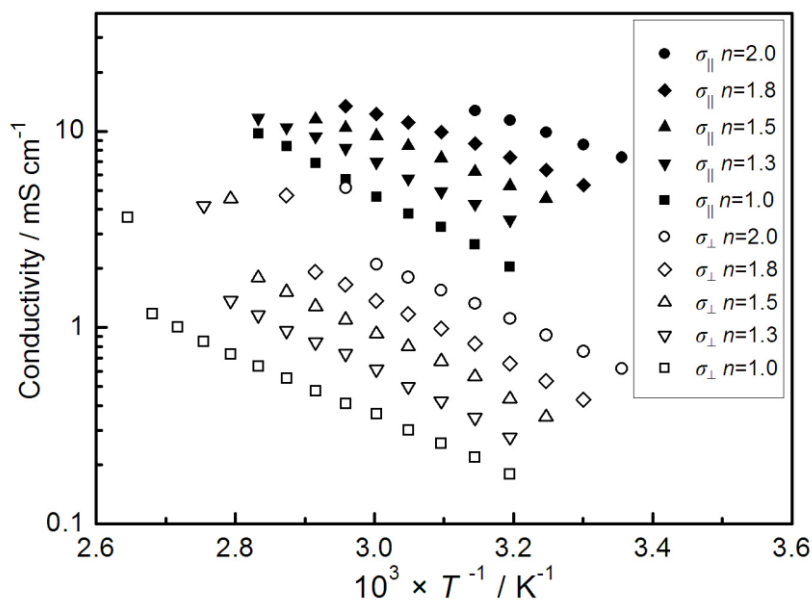


Figure 9. Temperature dependence of σ_{\parallel} and σ_{\perp} for $C_{12}MIm(FH)_nF$ ($n = 1.0, 1.3, 1.5, 1.8, \text{ and } 2.0$).

Figure 9 shows the temperature dependence of σ_{\parallel} and σ_{\perp} for $C_{12}\text{MIm}(\text{FH})_n\text{F}$ ($n = 1.0, 1.3, 1.5, 1.8,$ and 2.0) (see Table S3 for the σ_{\parallel} and σ_{\perp} values at each temperature). For all these $C_{12}\text{MIm}(\text{FH})_n\text{F}$ ILCs, σ_{\parallel} is about ten times higher than σ_{\perp} , suggesting that the ion mobility is higher within the ion-conductive layers than it is perpendicular to them. The increase in σ_{\parallel} and σ_{\perp} with increasing n value is due to the decrease in the cation-anion interaction, which leads to a higher ion mobility for the anions in the polar region. The degree of anisotropy in ionic conductivity is almost the same for the different n values ($\sigma_{\parallel}/\sigma_{\perp} \approx 10$), since the thickness of the insulating sheets formed by the dodecyl alkyl chains is not significantly changed. This is in contrast to the cases for $C_x\text{MIm}(\text{FH})_2\text{F}$ ($x = 10, 12, 14,$ and 16), which yield different anisotropy according to the different alkyl chain lengths.²¹ The discontinuous gap in σ_{\perp} at the clearing point results from the breakup of the layer structure. Since the cation is much larger than the anion and is linked to the adjacent cation by van der Waals interactions, the dominant charge carrier in the ion-conductive layer is thought to be $(\text{FH})_n\text{F}^-$. Such a conduction mechanism is preferred in electrochemical systems where diffusion of fluorohydrogenate ions is important in the electrode reactions. Moreover, $C_{12}\text{MIm}(\text{FH})_n\text{F}$ ($n = 1.0\text{--}1.3$) shows anisotropic ionic conductivity as high as 10 mS cm^{-1} around $80 \text{ }^\circ\text{C}$, which implies that these fluorohydrogenate ILCs can be used in high-temperature applications.

Conclusions

The thermal, structural, and ion-conductive properties of 1-dodecyl-3-methylimidazolium fluorohydrogenate ILCs, $C_{12}\text{MIm}(\text{FH})_n\text{F}$ ($n = 1.0\text{--}2.3$), were investigated. The ILCs have a smectic A interdigitated bilayer structure in the liquid crystalline mesophase, and the temperature range of the mesophase decreases with increasing n value. The layer spacing of the interdigitated bilayer structures decreases with increasing temperature or increasing n value in the liquid crystalline mesophase. A mixed crystal system was observed for $C_{12}\text{MIm}(\text{FH})_n\text{F}$ ($n = 1.0\text{--}2.3$) with two crystal structures (Type I, $1.0 \leq n < 1.9$, and Type II, $1.9 < n \leq 2.3$). The ionic conductivity increases with increasing n value both

parallel and perpendicular to the smectic ion-conductive layers, while the anisotropy is unchanged, since the thickness of the insulating sheet formed by the dodecyl alkyl chains does not change significantly.

Experimental

Apparatus and Materials. Volatile materials were handled in a vacuum line constructed of SUS316 stainless steel and PFA (tetrafluoroethylene-perfluoroalkylvinylether copolymer). Nonvolatile materials were handled under a dry Ar atmosphere in a glove box. The starting chloride, $C_{12}MImCl$, was prepared by equimolar reaction of 1-methylimidazole (Aldrich, 99%) and 1-chlorododecane (TCI-EP, 97%) at 80 °C for three days, as described in the literature.²¹ Purification of $C_{12}MImCl$ was performed by dissolving the salts in acetonitrile (dehydrated, Wako Chemicals, 99%) and then precipitating them from the solution by adding ethyl acetate (dehydrated, Wako Chemicals, 99.5%). Anhydrous HF (Daikin Industries) was dried over K_2NiF_6 prior to use.

Synthesis of $C_{12}MIm(FH)_{2.3}F$. The starting chloride, $C_{12}MImCl$, was charged into a PFA reactor under a dry Ar atmosphere, and a large excess of anhydrous HF was distilled onto it at -196 °C. The mixture reacted upon warming up to room temperature, and the volatile gases were roughly eliminated by evacuation using a rotary pump. Elimination of the volatile gases and addition of fresh HF were repeated to effectively eliminate chloride in the form of hydrogen chloride from the salt. Thorough evacuation at 25 °C resulted in $C_{12}MIm(FH)_{2.3}F$. The HF composition of the obtained salts was confirmed by elemental analysis and titration using aqueous 0.1029 M NaOH (see Table S1 for the results of the determination of the HF composition).

Synthesis of $C_{12}MIm(FH)_{1.0}F$. The chloride, $C_{12}MImCl$ (2.869 g, 10.00 mmol), was weighed and dissolved in 100 mL water. The aqueous solution was slowly added to a tube (50 cm long) filled with anion exchange resin (OH^- type, Dowex Monosphere 550A, Aldrich), and dropped down at a rate of one drop per second, after which 300 mL of water was added to wash out all the product. An HF (about 1 M) solution was added to the obtained $C_{12}MImOH$ solution until the pH reached 7.0. An equal amount of HF solution was added again to obtain the $C_{12}MImFHF$ solution, which was dried under vacuum up to 80 °C. The HF composition of the obtained salts was confirmed by elemental analysis and titration

using aqueous 0.1029 M NaOH (see Table S1 for the results of the determination of the HF composition).

Synthesis of $C_{12}MIm(FH)_nF$ ($n = 1.1-2.2$). Stoichiometric amounts of $C_{12}MIm(FH)_{1.0}F$ and $C_{12}MIm(FH)_{2.3}F$ were mixed and dissolved in acetonitrile, after which the solvent was removed under vacuum at room temperature. Elevation of the temperature was avoided, because it can lead to a decrease in the n value.

Analysis. Infrared spectra of solid and liquid samples were obtained using an FTS-165 (BIO-RAD Laboratories) instrument. The samples were sandwiched between a pair of AgCl crystal windows in a stainless steel cell. Thermogravimetric and DSC analyses were performed under a dry Ar gas flow using Shimadzu DTG-60H and Shimadzu DSC-60 instruments, respectively, at a scanning rate of $5\text{ }^\circ\text{C min}^{-1}$. The sample was placed in a Ni open cell for TG analysis and in a sealed stainless steel cell for DSC. Polarized optical microscopy was carried out using a VHX digital microscope (Keyence) under cross-polarized light at $\times 100$ magnification. The sample was placed in a transparent cell made of sapphire and covered with a piece of glass substrate. The temperature was controlled by a TS1500 hot stage unit (Japan High Tech). X-ray diffraction was performed using a Rigaku Ultima IV diffractometer ($\text{Cu K}\alpha$, $\lambda = 1.5418\text{ \AA}$) with an output power of 40 kV and 40 mA. The data were recorded in 2θ ranges of $2^\circ-6^\circ$ (scanning rate of 1° min^{-1}) and $2^\circ-30^\circ$ (scanning rate of 2° min^{-1}) with a step of 0.02° . The sample was sealed in an airtight cell made of acrylic resin with Kapton film windows. Heating and cooling rates of $5\text{ }^\circ\text{C min}^{-1}$ were used. The ionic conductivity was measured according to the AC impedance technique using a PARSTAT 2273 electrochemical measurement system (Princeton Applied Research). The ionic conductivities σ_{\parallel} and σ_{\perp} were measured according to the previously reported method.²¹ A pair of comb-shaped gold electrodes was used to measure σ_{\parallel} . Gold (*ca.* $0.8\text{ }\mu\text{m}$ in thickness) was deposited on the glass substrate in a comb shape after deposition of indium tin oxide (ITO) (*ca.* $0.1\text{ }\mu\text{m}$) in this pattern to reinforce the contact to the glass. The sample was placed in the comb-shaped region and covered with a piece of glass substrate to help the alignment. A pair of ITO glass electrodes was used to measure the conductivity perpendicular to smectic layer, σ_{\perp} . The sample was sandwiched with two ITO glass

electrodes and fixed with a Teflon spacer (50 μm in thickness) with a hole in the center (3 mm i.d.). The cell constants of these cells were calibrated with a KCl aqueous solution (0.747 g kg^{-1}), EMImBF₄ (Kanto Kagaku), and BMImPF₆ (Kanto Kagaku). These conductivity measurement cells were placed in an airtight cell to avoid the effects of moisture in air. The cell was held at each temperature for more than one hour to obtain a steady resistance, and the measurement was repeated several times to confirm the reproducibility of the data. No etching of the glass surface was observed after the measurement.

Acknowledgements

This work was financially supported by a Grant-in-Aid for Scientific Research of the Japan Society for the Promotion of Science, #20246140.

Supporting Information Available: Results of elemental analysis and titration, ionic conductivities, IR spectra, TG analysis, DSC results, POM results, and XRD data. These materials are available free of charge via the Internet at <http://pubs.acs.org>.

References

- (1) Binnemans, K. *Chem. Rev.* **2005**, *105*, 4148–4204.
- (2) Yoshio, M.; Mukai, T.; Ohno, H.; Kato, T. *J. Am. Chem. Soc.* **2004**, *126*, 994–995.
- (3) Yoshio, M.; Kagata, T.; Hoshino, K.; Mukai, T.; Ohno, H.; Kato, T. *J. Am. Chem. Soc.* **2006**, *128*, 5570–5577.
- (4) Shimura, H.; Yoshio, M.; Hoshino, K.; Mukai, T.; Ohno, H.; Kato, T. *J. Am. Chem. Soc.* **2008**, *130*, 1759–1765.
- (5) Yoshio, M.; Mukai, T.; Kanie, K.; Yoshizawa, M.; Ohno, H.; Kato, T. *Adv. Mater.* **2002**, *14*, 351–354.
- (6) Mukai, T.; Yoshio, M.; Kato, T.; Yoshizawa, M.; Ohno, H. *Chem. Commun.* **2005**, 1333–1335.
- (7) Yamanaka, N.; Kawano, R.; Kubo, W.; Kitamura, T.; Wada, Y.; Watanabe, M.; Yanagida, S. *Chem. Commun.* **2005**, 740–742.
- (8) Lee, C. K.; Huang, H. W.; Lin, I. J. B. *Chem. Commun.* **2000**, 1911–1912.
- (9) Hagiwara, R.; Hirashige, T.; Tsuda, T.; Ito, Y. *J. Fluorine Chem.* **1999**, *99*, 1–3.
- (10) Hagiwara, R.; Hirashige, T.; Tsuda, T.; Ito, Y. *J. Electrochem. Soc.* **2002**, *149*, D1–D6.
- (11) Matsumoto, K.; Hagiwara, R.; Ito, Y. *Electrochem. Solid-State Lett.* **2004**, *7*, E41–E44.
- (12) Matsumoto, K.; Hagiwara, R. *Electrochemistry* **2005**, *73*, 730–732.
- (13) Hagiwara, R.; Nohira, T.; Matsumoto, K.; Tamba, Y. *Electrochem. Solid-State Lett.* **2005**, *8*, A231–A233.
- (14) Kanematsu, S.; Matsumoto, K.; Hagiwara, R. *Electrochem. Commun.* **2009**, *11*, 1312–1315.
- (15) Senda, A.; Matsumoto, K.; Nohira, T.; Hagiwara, R. *J. Power Sources* **2010**, *195*, 4414–4417.
- (16) Yamagata, M.; Konno, S.; Matsumoto, K.; Hagiwara, R. *Electrochem. Solid-State Lett.* **2009**, *12*, F9–F12.
- (17) Ohtsuki, J.; Matsumoto, K.; Hagiwara, R. *Electrochemistry* **2009**, *77*, 624–626.
- (18) Enomoto, T.; Nakamori, Y.; Matsumoto, K.; Hagiwara, R. *J. Phys. Chem. C* **2011**, *115*, 4324–4332.
- (19) Taniki, R.; Matsumoto, K.; Hagiwara, R. *Electrochem. Solid-State Lett.* **2012**, *15*, F13–F15.

- (20) Lee, J.; Nohira, T.; Hagiwara, R. *J. Power Sources* **2007**, *171*, 535–539.
- (21) Xu, F.; Matsumoto, K.; Hagiwara, R. *Chem. Eur. J.* **2010**, *16*, 12970–12976.
- (22) Xu, F.; Matsubara, S.; Matsumoto, K.; Hagiwara, R. *J. Fluorine Chem.*, **2012**, *135*, 344–349.
- (23) Fuchigami, T. *J. Fluorine Chem.* **2007**, *128*, 311–316.
- (24) Hagiwara, R.; Nakamori, Y.; Matsumoto, K.; Ito, Y. *J. Phys. Chem. B* **2005**, *109*, 5445–5449.
- (25) Tani, Y.; Nohira, T.; Enomoto, T.; Matsumoto, K.; Hagiwara, R. *Electrochim. Acta*, **2011**, *56*, 3852–3856.
- (26) Hagiwara, R.; Matsumoto, K.; Nakamori, Y.; Tsuda, T.; Ito, Y.; Matsumoto, H.; Momota, K. *J. Electrochem. Soc.* **2003**, *150*, D195–D199.
- (27) Saito, Y.; Hirai, K.; Matsumoto, K.; Hagiwara, R.; Minamizaki, Y. *J. Phys. Chem. B* **2005**, *109*, 2942–2948.
- (28) Gennick, I.; Harmon, K. M.; Potvin, M. M. *Inorg. Chem.* **1977**, *16*, 2033–2040.
- (29) Clark, J. H.; Emsley, J.; Jones, D. J.; Overrill, R. E. *J. Chem. Soc. Dalton Trans.* **1981**, 1219–1222.
- (30) Chandler, W. D.; Johnson, K. E.; Campbell, J. L. E. *Inorg. Chem.* **1995**, *34*, 4943–4949.
- (31) Rosenvinge, T. V.; Parrinello, M.; Klein, M. L. *J. Chem. Phys.* **1997**, *107*, 8013–8019.
- (32) Bowlas, C. J.; Bruce, D. W.; Seddon, K. R. *Chem. Commun.* **1996**, 1625–1626.
- (33) Gordon, C. M.; Holbrey, J. D.; Kennedy, A. R.; Seddon, K. R. *J. Mater. Chem.* **1998**, *8*, 2627–2636.
- (34) Holbrey, J. D.; Seddon, K. R. *J. Chem. Soc. Dalton Trans.* **1999**, 2133–2139.
- (35) Xu, F.; Matsumoto, K.; Hagiwara, R. *Dalton Trans.* **2012**, *41*, 3494–3502.
- (36) Dierking, I. *Textures of Liquid Crystals*; WILEY-VCH: Weinheim, Germany, 2003.
- (37) Axenov, K. V.; Laschat, S. *Materials* **2011**, *4*, 206–259.
- (38) Bradley, A. E.; Hardacre, C.; Holbrey, J. D.; Johnston, S.; McMath, S. E. J.; Nieuwenhuyzen, M. *Chem. Mater.* **2002**, *14*, 629–635.
- (39) Forrester, J. D.; Templeton, D. H.; Zalkin, A.; Senko, M. E. *Acta Crystallogr.* **1963**, *16*, 58–62.
- (40) Mootz, D.; Boenigk, D. *J. Am. Chem. Soc.* **1986**, *108*, 6634–6636.
- (41) Matsumoto, K.; Tsuda, T.; Hagiwara, R.; Ito, Y.; Tamada, O. *Solid State Sci.* **2002**, *4*, 23–26.

